Correspondence to:

J. Labidi,
labidi@ipgp.fr

Clumped Isotope Signatures of Abiotic Methane: The Role of the Combinatorial Isotope Effect

Jabrane Labidi[1] , **Thomas M. McCollom[2]**, **Thomas Giunta[3]**, **Barbara Sherwood Lollar[1,4]**, **William D. Leavitt[5,6]** , and **Edward D. Young[7]**

[1]Institut de Physique du Globe de Paris, CNRS, Université de Paris Cité, Paris, France, [2]Laboratory for Atmospheric and Space Physics, University of Colorado, Boulder, CO, USA, [3]CNRS, Ifremer, Geo-Ocean, University of Brest, Plouzané, France, [4]Department of Earth Sciences, University of Toronto, Toronto, ON, Canada, [5]Department of Earth Sciences, Dartmouth College, Hanover, NH, USA, [6]Department of Chemistry, Dartmouth College, Hanover, NH, USA, [7]Department of Earth, Planetary, and Space Sciences, UCLA, Los Angeles, CA, USA

Abstract Methane clumped isotope signatures of abiogenesis may be diagnostic of the origin of methane on Earth and other planetary bodies. We performed synthesis of abiogenic methane in hydrothermal conditions between 130 and 300°C and determined $\delta^{13}C$, δD, $\Delta^{13}CH_3D$, and $\Delta^{12}CH_2D_2$. The experiments were performed by heating water in the presence of Fe^0 powder and CO. The reduction of water on metallic iron led to the formation of H_2. CO was reacted with both H_2 and H_2O, generating both CH_4 and CO_2. Methane $\delta^{13}C$ values are isotopically depleted by ~25‰ relative to the CO starting material. This is consistent with carbon isotopic equilibrium between methane, carbon monoxide and carbon dioxide in our experiments. In contrast, D/H ratios are inconsistent with equilibrium isotopic fractionation, as illustrated by δD values of methane fractionated by ~500‰ relative to starting H_2O. This suggests that under our experimental conditions, hydrogen additions to carbon may be governed by kinetics. $\Delta^{13}CH_3D$ values track experimental temperature, with values between +1.5‰ and +5.0‰ for most samples. In contrast, $\Delta^{12}CH_2D_2$ values are displaced from equilibrium. We find exclusively negative $\Delta^{12}CH_2D_2$ values, showing deficits down to 40‰ relative to thermodynamic equilibrium. We interpret the data as evidence for distinct, kinetically induced D/H pools contributing to methane assembly, that is, a combinatorial effect. The cumulative D/H fractionations associated with CO hydrogenation explain the direction and magnitude of $\Delta^{12}CH_2D_2$ values during abiotic methane formation. We suggest that near equilibrium $\Delta^{13}CH_3D$ with negative $\Delta^{12}CH_2D_2$ signatures will help identify methane formed abiotically in nature.

Plain Language Summary Methane is observed in various environmental settings on Earth, including but not limited to, hydrothermal fluids and sedimentary systems. It is also found on other worlds, as it was reported to occur on Mars, in Enceladus's geysers, and as of recently, in an exoplanet's atmosphere. Methane may be formed by life or by non-biological processes, so the presence of methane alone on another world is not enough to declare a planet habitable. Geochemists have built methods to tell biogenic from abiotic methane, which ought to be useful for the identification of life-derived methane on another planet. Those techniques are crucial but complex, based on integrated studies combining molecular and isotopic compositions of methane and associated gases. Here, we report on whether abiotic methane shows a unique signature for $^{13}CH_3D$ and $^{12}CH_2D_2$, the mass-18 isotopologues of methane. We performed synthesis of abiotic methane in the laboratory and determined its composition. We observe unique signatures for methane clumping, where $^{12}CH_2D_2$ disequilibrium is associated with equilibrium $^{13}CH_3D$ abundances. We suggest that near equilibrium $\Delta^{13}CH_3D$ with negative $\Delta^{12}CH_2D_2$ signatures will help identify methane formed abiotically on Earth and on other worlds.

1. Introduction

Methane (CH_4) is observed in a variety of environments on Earth. It is a minor component on the surfaces of many planets and planetesimals from our solar system, such as on Mars and Enceladus. In planetary environments, methane may be abiotic, that is, synthesized by mechanisms that do not involve life or thermal decomposition of organic matter. Reaction 1 is central for the abiotic synthesis of methane on planetary surfaces and at depth:

$$CO_2 + 4H_2 = CH_4 + 2H_2O. \tag{1}$$

Reaction 1 may occur in hydrothermal systems, where olivine-rich ultramafic rocks are altered via serpentinization reactions to produce abundant H_2. The synthesis of H_2 allows reaction 1 to proceed abiotically at temperatures under 340°C (Klein et al., 2019). Formally, reaction 1 is the Sabatier reaction, although it is often lumped with a class of reactions referred to as Fischer-Tropsch-Type synthesis, or FTT, as reviewed elsewhere (McCollom, 2013; McCollom & Seewald, 2007). Alternatively, methane may be synthesized biologically. Three metabolic pathways of methane synthesis exist on Earth, all proceeding at temperatures typically less than 90°C (Head et al., 2003), although microbial methanogenesis at temperatures up to ~120°C has been found viable in the laboratory (Takai et al., 2008). First, hydrogenotrophic methanogens perform reaction 1 in environments where CO_2 and H_2 substrates are available (Fenchel et al., 2012). The hydrogenotrophic pathway has been hypothesized to be relevant to any past life on Mars (Sauterey et al., 2022) and could be feasible on other terrestrial planets, sustained by the ubiquity of CO_2 + H_2 (Thompson et al., 2022). Two other pathways, methylotrophic and acetotrophy methanotrophy, may occur in environments where methylated and acetate substrates are available (Fenchel et al., 2012).

Biosignatures have been a long-term focus of investigation. They correspond to a compound, isotopic signature or pattern that life is known to produce. The veracity of a potential biosignatures comes not only from the potential of life having produced it, but also from the improbability of non-biological processes producing a "false positive" (NASEM, 2022; Neveu et al., 2018). Thus, experimental consideration of potential abiosignatures has been flagged as a critical gap in the search for life beyond Earth. A means for identifying abiotic methane is therefore desirable given the importance of methane in the search for life on other worlds. Geochemists have documented contributions of abiotic methane to terrestrial environments using multiple approaches, including field observations, microbiology and stable isotope geochemistry of methane and co-existing gases (Etiope & Sherwood Lollar, 2013; Etiope & Whiticar, 2019). Abiotic CH_4 is thought to occur in seafloor hydrothermal fluids vented at temperatures typically exceeding 250°C (Charlou et al., 2010; Welhan & Craig, 1979), and in lower-temperature hydrothermal vent fluids, like at Lost City (Kelley et al., 2005). At Lost City, methane is thought to be mainly abiotic in origin, but includes contributions of microbial gas (Bradley & Summons, 2010; Proskurowski et al., 2008). Abiotic methane is thought to be produced in continental seeps, springs, and fracture waters in the subsurface, at environmental temperatures typically ≤100°C (Etiope & Sherwood Lollar, 2013). It is found in fluids from Precambrian rocks worldwide including the Kidd Creek mine, Canada (Etiope et al., 2015; Fritz et al., 1992; Sherwood Lollar et al., 1993, 2002, 2008) and sites on the Fennoscandian Shield (Kietäväinen & Purkamo, 2015) and Southern Africa (Sherwood Lollar et al., 2006). It is also suspected to occur in fluids issued from the Oman ophiolite with larger additions of microbial sources, although debate persists (Etiope et al., 2015; Miller et al., 2016; Nothaft et al., 2021).

Here, we discuss methane isotope clumping as a potential tool to more clearly identify abiotic methane on Earth and elsewhere. We use the abundances of doubly-substituted mass-18 methane isotopologues of methane, $^{13}CH_3D$ and $^{12}CH_2D_2$. The doubly-substituted isotopologues are often referred to as "clumped isotopes" to reflect that each molecule contains two of the less abundant isotopes. Methane clumped isotopes have been used as tracers of methane origin in nature (Douglas et al., 2017; Giunta et al., 2019; Labidi et al., 2020; Lalk et al., 2022; Liu et al., 2024; Stolper et al., 2014; D. T. Wang et al., 2015; Young et al., 2017). The potential for $\Delta^{12}CH_2D_2$ and $\Delta^{13}CH_3D$ to demonstrate abiogenicity of natural methane on Earth and other worlds is illustrated by preliminary experimental work. So far, two Sabatier-type experimental runs have been investigated for $\Delta^{13}CH_3D$ versus $\Delta^{12}CH_2D_2$ (Young et al., 2017). Those methane aliquots were generated by CO_2 reduction (reaction 1) catalyzed by ruthenium at 70 and 90°C following the method of Etiope and Ionescu (2015). The experiments yielded near-equilibrium $\Delta^{13}CH_3D$ values of ~+4‰, but large $^{12}CH_2D_2$ depletions of approximately 70‰ relative to equilibrium. These empirical values have been thought to reflect a signature acquired by methane during the abiotic reduction of oxidized carbon in the laboratory and potentially in nature (Young et al., 2017).

The Sabatier experiments reported in Young et al. (2017) were performed at temperatures below 100°C and in the absence of water. These experimental conditions are challenging to extrapolate to deep-sea hydrothermal systems or continental environments relevant for the search of abiotic methane on Earth and on other worlds. Consequently, it is not clear how the experimental data should be applied to the interpretation of natural systems. To constrain the $\Delta^{12}CH_2D_2$ and $\Delta^{13}CH_3D$ signatures produced by abiotic FTT reactions at variable temperatures, we performed controlled FTT synthesis at hydrothermal conditions in the laboratory at temperatures varying between 130 and 300°C.

2. Experiments

The experimental methods employed follow those used previously to study abiotic methane and other organic syntheses by Fischer-Tropsch-type (FTT) reactions under hydrothermal conditions (McCollom & Seewald, 2006; McCollom et al., 2010). Briefly, a flexible-cell reaction cell composed of a gold bag with titanium fittings is contained inside a stainless-steel pressure housing (Seyfried et al., 1987). An external valve connected to the reaction cell with titanium tubing allowed for collection of volatile gases at the end of the experiments. Prior to the experiments, the internal reaction cell components were heated for 2 hours at 450°C in air to remove organic contaminants and to create an inert TiO_2 layer on the surface of the titanium fittings. Previous experiments with the same reaction system have demonstrated that the reactor itself is not catalytic for organic synthesis under the experimental conditions (McCollom & Seewald, 2006; McCollom et al., 2010; Seewald et al., 2006).

The experiments were performed by heating carbon monoxide (CO) and native iron (Fe^0) in the presence of water at a range of temperatures. The experiments were initiated by placing 1.5 g of Fe^0 (Fe powder, −22 mesh; Alfa Aesar) and ∼25 g of DI water in a 55 mL gold reaction cell. The metallic Fe is included both as catalyst for methane synthesis but also as a reactant for the generation of molecular hydrogen (H_2) since it rapidly reacts with water at elevated temperatures to form magnetite (Fe_3O_4) and H_2 according to the reaction:

$$3Fe^0 + 4H_2O \rightarrow Fe_3O_4 + 4H_2. \tag{2}$$

To promote reaction of Fe^0, the water was acidified to a pH of about 2 with HCl. Individual experiments were conducted over a range of temperatures from 130 to 300°C. The target pressure for the experiments was 15 MPa, but in practice the pressures varied up to 3 MPa from this value during some experiments.

After sealing the reaction cell with the Ti closure piece, it was placed in the pressure containment vessel, pressurized at room temperature, and the entire apparatus was placed horizontally and heated in a furnace. Once the target temperature was attained, CO was injected through the sampling valve using the following procedure. First, a loop of stainless-steel tubing (12.6 mL) was filled with CO at a pressure of 0.93 MPa (the maximum allowed by the pressure regulator on the CO tank) and attached to the sampling valve. A solution with the same composition as that in the reaction cell was then pumped into the tubing until pressure was equal to that within the heated pressure vessel. The valve was then opened and the CO along with 13 mL of solution was pumped into the reaction cell, with an equal amount of water bled from the pressure containment vessel to maintain constant pressure during injection. In practice, some amount of CO remained in the injection loop after this procedure, so it is not possible to determine exactly how much CO was contained in the reaction cell following injection. However, assuming 90% injection efficiency, the amount of CO injected would have been about 4.3 mmol. Considering that 38 mL of water (25 mL initial + 13 mL added during injection) corresponds to ∼2.1 mol H_2O, the starting CO/H_2O is estimated to be approximately 2×10^{-3}. Considering the 1.5 g of Fe^0, the Fe/H_2O molar ratios in the reaction cell was ∼1.25×10^{-2}.

The tank of CO used in the experiments was the same as that used in McCollom et al. (2010) and has a $\delta^{13}C$ of −28‰ V-PDB. The water used in this study is deionized water purified from Boulder, Colorado tap water. The δD of DI water sampled in April 2022 and April 2023 was −119‰ V-SMOW, similar to measurements of Boulder tap water measured in older studies (−116‰ ± 1‰; Landwehr et al., 2014). The molecular hydrogen (H_2) generated from reaction 2 subsequently reacts with CO to form methane, according to the net reaction:

$$CO + 3H_2 = CH_4 + H_2O \tag{3}$$

Reaction 3 is a FTT reaction that utilizes CO for oxidized carbon rather than CO_2. It is distinct from the Sabatier reaction (reaction 1) that may be similar to reactions in natural hydrothermal systems where CO_2 is available in large amounts. Carbon monoxide was used here because it is more active in hydrothermal FTT reactions than CO_2 (McCollom et al., 2010), which allowed for obtaining measurable CH_4 quantities under our experimental timescales. In addition to CO reduction, the so-called "water-gas shift reaction" (McCollom & Seewald, 2006; Seewald et al., 2006) is prominent under the experimental conditions; reaction between CO and water leads to the oxidation of a fraction of the CO to form CO_2:

$$CO + H_2O = CO_2 + H_2. \tag{4}$$

Through a competition between reactions 3 and 4, CO is rapidly and predominantly converted to CH_4 and CO_2, with much of the CO_2 precipitating as siderite ($FeCO_3$). Reaction 4 is anticipated to be dominant over reaction 3 (McCollom & Seewald, 2006; McCollom et al., 2010; Seewald et al., 2006).

The experiments were heated for 18–138 hr, with longer incubation times used at lower temperatures to allow for the synthesis reactions to proceed. Following reaction, the reactors were gradually cooled to room temperature while pumping water into the containment vessel to maintain elevated pressure. The pressure was then reduced to ∼5 MPa by releasing water from the pressure containment vessel in order to allow volatile gases to exsolve and accumulate at the top of the internal gold-titanium reaction cell. Within 24 hr of experiment termination, the gas phase was vented through the sampling valve and transferred to 300 mL stainless steel cylinders (Swagelok) for isotope analysis.

3. Isotope Measurements

Methane was extracted from the stainless-steel storage cylinders on a vacuum system at UCLA and purified by gas chromatography using procedures described previously by Young et al. (2017). Gas aliquots of a given sample were opened to a silica gel-filled stainless-steel U-trap cooled with liquid nitrogen. Helium carrier gas was used to flush the sample to the gas chromatograph. Separation was accomplished with a 3 m long, 1/8 in. OD stainless steel column packed with 5 Å molecular sieve, followed in series by a 2 m long · 1/8 in. OD stainless steel column packed with HayeSep D porous polymer. Peaks from the gas chromatograph were detected with an in-line thermal conductivity detector. Because total pressures were >1 bar in the reaction vessels, and because samples were dominated by H_2, purification on the vacuum line had to be performed in sequence of multiple aliquots. Once collection of a purified aliquot of methane was complete, this methane was transferred to a glass vial filled with silica-gel at liquid nitrogen temperature. Another sample aliquot would then be purified and added to the same glass vial, until a given sample cylinder had been entirely processed. For the cylinders to be emptied, 6–8 aliquots were processed in this way on the vacuum line. Samples were then transferred to the inlet of the mass spectrometer where they were warmed and expanded into the mass spectrometer using a silica-gel filled cold finger.

Mass spectrometry measurements were done on a Nu Instruments Panorama with a mass resolving power that allows the simultaneous measurement of ion currents for resolved $^{12}CH_4^+$, $^{13}CH_4^+$, $^{12}CH_3D^+$, $^{13}CH_3D^+$, and $^{12}CH_2D_2^+$ ion beams, as described in Young et al. (2016). The analyte peaks are in most cases baseline resolved from surrounding interferences, and where there is the potential for a tail effect (in the case of $^{13}CH_5^+$ tailing into $^{12}CH_2D_2^+$), previous work shows that the effects on our final results are less than quoted uncertainties (Young et al., 2016). The measured ratios of these ion currents yield values for both $\Delta^{13}CH_3D$ and $\Delta^{12}CH_2D_2$ as well as for bulk $^{13}C/^{12}C$ and D/H. The methane quantities available for isotopic measurements were relatively low. For standards and samples available in quantities >80 µmol, relative abundances of $^{13}CH_3D^+$ and $^{12}CH_2D_2^+$ are measured for up to 10 and 20 hr, respectively. In these cases, typical propagated internal uncertainties for the calculation of $\Delta^{13}CH_3D$ and $\Delta^{12}CH_2D_2$ are generally ±0.1‰ and ±0.5‰, respectively. In our study, often only 35–60 µmol of CH_4 were available (Table 1), and uncertainties are larger, reflecting less favorable counting statistics. The internal uncertainties range from 0.2‰ to 0.5‰ for $\Delta^{13}CH_3D$, and between 1.1‰ and 3.2‰ for $\Delta^{12}CH_2D_2$.

4. Results

For nine experiments conducted at temperatures between 130 and 300°C, between ∼5 and ∼80 µmol of abiotic CH_4 were obtained. All results may be found in Table 1 and online via the EarthChem repository (Labidi et al., 2024). The 7 experiments done at temperatures equal to or lower than 250°C yielded more than 35 µmoles CH_4, enough for isotopic measurements. The δD of their product methane vary between −583‰ and −608‰ versus V-SMOW (Figure 2), much lower than the starting δD of water (−119‰). Hydrogen isotope ratios of methane are positively correlated with temperatures (Figure 2). At the highest temperatures, the hydrogen isotope composition of methane tends to be the most enriched in D. A clear outlier to this trend is FT18-4, the experiment conducted at the lowest temperature (130°C), which shows the highest δD of the series (−582‰). The δD values for the methane synthesized in this study are different from those obtained in McCollom et al. (2010) (with values of ∼−550‰) although experimental conditions except for temperature were similar. We attribute the small differences as the simple reflection of variable starting water for the experiments: in the study of McCollom

Table 1
Methane Isotope Data for Synthesized Abiotic Methane

	FT17-1	FT18-1	FT18-2	FT18-3	FT18-4	FT18-5	FT19-7	FT19-8	FT20-1
Temperature (°C)	250	246	211	170	132	183	300	185	275
Duration (hr)	24	14	89	90	139	67	19	139	18
Micromoles CH_4	35	40	50	65	75	79	1	75	10
$\delta^{13}C$ PDB	−55.3	−58.3	−61.7	−51.5	−44.1	−56.4		−55.3	
δD SMOW	−583	−592	−597	−608	−583	−605		−608	
$\Delta^{13}CH_3D$	2.0	1.7	2.1	5.8	4.8	2.0		3.9	
1 se	0.5	0.4	0.3	0.2	0.2	0.3		0.3	
$\Delta^{12}CH_2D_2$	−11.7	−9.9	−3.0	−29.0	−30.3	−32.1		−27.0	
1 se	3.2	2.0	2.4	1.5	1.1	1.6		2.5	

Note. Bulk $^{13}C/^{12}C$ and D/H are reported alongside $\Delta^{13}CH_3D$ and $\Delta^{12}CH_2D_2$. Analytical uncertainties are below 0.1‰ (95% confidence intervals) for $\delta^{13}C$ and δD. Propagated uncertainties are listed for $\Delta^{13}CH_3D$ and $\Delta^{12}CH_2D_2$ in 1σ. They are highly variable and directly reflect counting statistics, that is, CH_4 quantity.

et al. (2010), the reactant water was purchased from Fischer®. The measured $\delta^{13}C$ of methane varies between −44‰ and −62‰ versus V-PDB (Figure 2). The carbon isotope values obtained here are similar to previous results obtained using the same experimental procedures and starting CO (McCollom et al., 2010). The $\delta^{13}C$ values are weakly correlated with temperature but interpretations of the correlation should be regarded with caution, considering the importance of FT18-4, the one outlier on Figure 2b.

We find $\Delta^{13}CH_3D$ values between 1.7‰ ± 0.4‰ (1σ, at 250°C) and 4.8‰ ± 0.2‰ (1σ, at $^{13}0$°C) for all experiments except one outlier, FT18-3, with a $\Delta^{13}CH_3D$ of 5.8‰ ± 0.2‰ (1σ, at 170°C). Most of the $\Delta^{13}CH_3D$ values track the temperature of abiotic methane synthesis within 1‰ (Figure 3a). In contrast with $\Delta^{13}CH_3D$, $\Delta^{12}CH_2D_2$ values are exclusively negative, ranging from −3.0‰ ± 2.5‰ (1σ) at 210°C to −32.0‰ ± 1.6‰ (1σ) at 183°C (Figure 3b). The negative $\Delta^{12}CH_2D_2$ values indicate that the relative amount of $^{12}CH_2D_2$ among methane isotopologues is lower than predicted for a stochastic gas equilibrated at $T > 1,000$°C. The $\Delta^{12}CH_2D_2$ values are positively correlated with peak experimental temperatures (Figure 3b); the magnitude of the disequilibrium relative to stochastic is greatest at the lowest temperatures.

5. Discussion

5.1. Experimental Synthesis of Abiotic Methane

Previous experimental studies of abiotic synthesis under hydrothermal conditions have shown that mineral reactants can introduce small amounts of background hydrocarbons that can potentially interfere with interpretation of the results. This is because organic reaction products in many studies are generated at low levels relative to background contaminants (e.g., Foustoukos & Seyfried, 2004; Fu et al., 2007; McCollom & Seewald, 2001, 2006, 2007). For instance, pioneer hydrothermal experiments involving CO_2 reduction associated with olivine serpentinization were performed at 300°C (Berndt et al., 1996). The authors observed the formation of substantial amounts of methane and other alkanes, which they attributed to the FTT synthesis of hydrocarbons by the reduction of dissolved CO_2. McCollom and Seewald (2001) performed a similar serpentinization experiment, but used a ^{13}C-labeled inorganic carbon source (>99% $NaHCO_3$) to trace the source of organic products. They found that <20% of the methane observed in the experiment was generated by reduction of the labeled carbon source, indicating that most of the observed methane and other hydrocarbons was contributed by background sources and that FTT reduction of dissolved CO_2 is more limited than suggested by Berndt et al. (1996).

Several considerations, however, indicate that background sources did not make a significant contribution to the methane observed in our experiments, and that the methane we measured was predominantly produced by abiotic synthesis. First, the Fe^0 included in the experiments is a highly effective catalyst for methane synthesis, and produced yields far higher than experiments performed with other, less-catalytic minerals present. As a result, the large methane yields would largely swamp out any small extraneous contributions derived from the reactants. Second, a similar previous FTT experiment performed with a ^{13}C-labeled carbon source (>99% $H^{13}COOH$) found
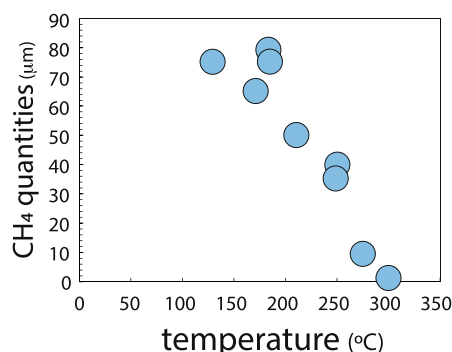
Figure 1. Quantities of synthesized abiotic methane versus temperature. Data display a negative trend with experiment temperature. See text for details. Note: there are nine samples here, but only seven for isotope measurements. The two highest temperatures did not yield enough methane for mass spectrometry.

that only small fraction of the methane generated could have come from background sources (McCollom & Seewald, 2006). That experiment was performed in the same laboratory using similar methods and an identical reaction apparatus with Fe^0 included as a catalyst, and the results indicated that >97% of the methane resulted from abiotic reduction of the labeled carbon source (i.e., >97% $^{13}CH_4$). Third, in two control experiments performed by McCollom et al. (2010) that included only Fe^0 and water with no added carbon source, again performed in the same laboratory with very similar methodology and identical reaction apparatus to the present study, only trace amounts of methane were generated (<3 μmoles CH_4). This amount is far below the methane yields from all but the highest temperature experiments in the present study (Figure 1). The correlation between decreasing methane yields and increasing temperature apparent in Figure 1 is an additional evidence against substantial contributions of background methane. There is no physical reason that background sources would contribute methane in larger amounts at lower temperatures than at higher temperatures, as observed on Figure 1.

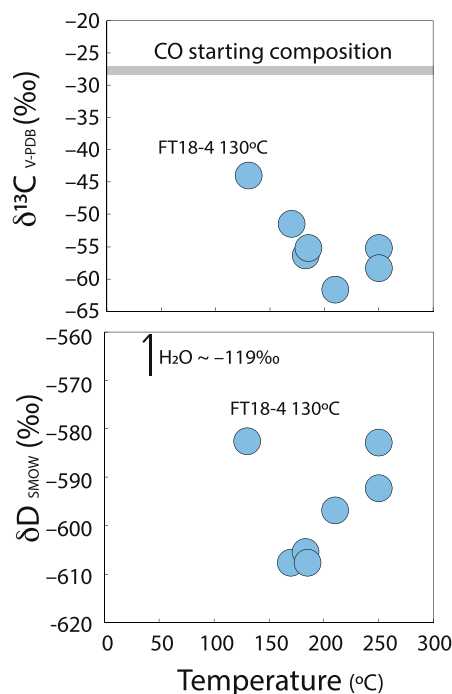**Figure 2.** $\delta^{13}C$ (panel a) and δD (panel b) of synthesized abiotic methane versus temperature and observed methane concentrations. $\delta^{13}C$ data display a weak negative trend with experiment temperature. See text for details.
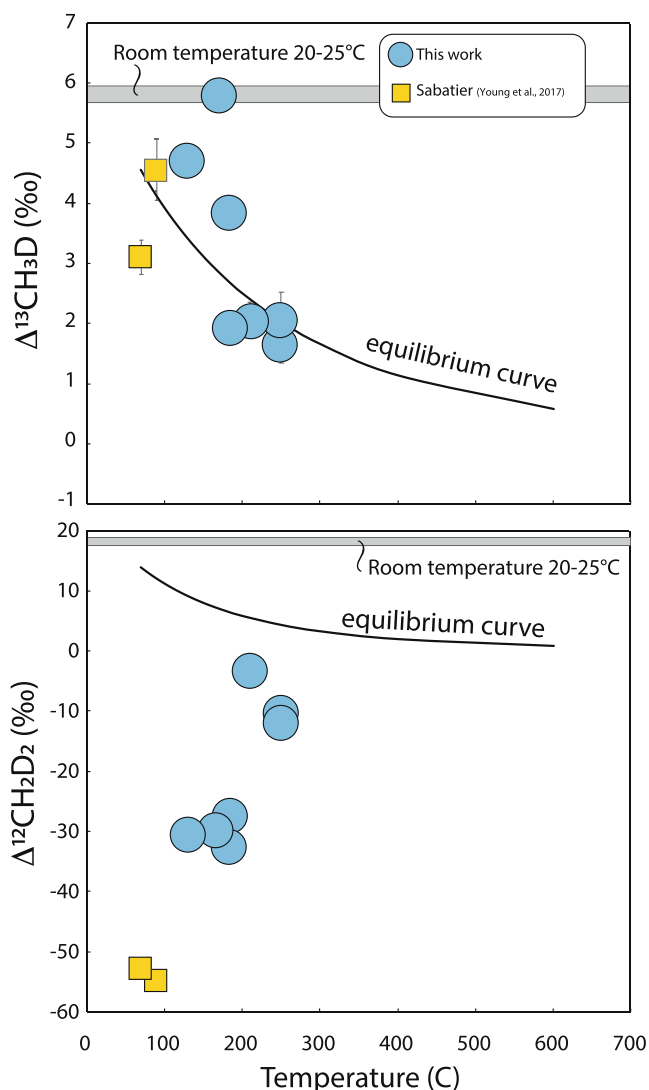
Figure 3. Relationships between the two mass-18 isotopologues of methane in experimental samples and the peak experimental temperatures. Data from other methane synthesized abiotically from Young et al. (2017) are also shown. Data and uncertainties are from Table 1.

Collectively, these considerations indicate that background sources contributed no more than a small fraction of the methane observed in our experiments, and that the methane in the experiments performed at 250°C or below was derived predominantly from abiotic reduction of CO.

The relationship on Figure 1 likely reflects the lifetime of the CO in hydrothermal experiments. Upon CO injection, conversion to CO_2 through reaction 4 begins, which competes with the sluggish reduction of CO to CH_4. According to Seewald et al. (2006), the half-time of CO oxidation to CO_2 in hydrothermal experiments is ~15 min at 300°C, longer than 1 day at 200°C, and almost 60 days at 130°C. This means that in our experiments conducted at $T > 250$°C, CO conversion to CO_2 likely happened so rapidly that very little FTT-derived methane is generated. Conversely, in experiments conducted at 250°C and below, for durations from under one day, up to almost 6 days, CO was present in the reaction chamber long enough to undergo reduction to methane.

5.2. The Carbon Isotope Balance in Our Experiments

The $\delta^{13}C$ signatures of methane vary around a value of $-55‰$ (V-PDB), with FT18-4 as the one outlier with a $\delta^{13}C$ of $-44‰$ (Figure 2). All methane samples have depleted $\delta^{13}C$ compared to the starting CO ($-28‰$). The isotopic difference of ~25‰ between CH_4 and the starting CO likely reflects $^{13}C/^{12}C$ fractionation during methane synthesis. Kueter et al. (2019) determined the equilibrium $^{13}C/^{12}C$ fractionations between CO, CO_2 and CH_4 at various temperatures between 1,200 and 300°C. At 300°C, the equilibrium $^{13}C/^{12}C$ fractionation between CO and CH_4 is $-3.1‰$, meaning that CH_4 should be enriched in ^{13}C relative to CO by 3.1‰. This is at odds with our observation of a ~25 to ~40‰ depletion in $^{13}C/^{12}C$ for CH_4 relative to the initial reactant CO. Instead, methane $\delta^{13}C$ values are broadly consistent with an approach to $^{13}C/^{12}C$ equilibrium between methane and CO_2. This implies that the synthesis of CO_2 from CO oxidation via reaction 4 was nearly quantitative so that CO_2 had nearly the same $^{13}C/^{12}C$ as the initial CO reactant ($-28‰$). Subsequent $^{13}C/^{12}C$ equilibration between CH_4 and this CO_2 would yield methane with a 25‰ ^{13}C depletion relative to CO_2 at 250°C, and roughly 40‰ at 150°C (Kueter et al., 2019), corresponding to predicted methane $\delta^{13}C$ values of $\sim-53‰$ and $-68‰$ at 250 and 150°C, respectively. This data supports near-complete conversion of CO to CO_2 and complete equilibration between CH_4 and CO_2. While imperfect, the magnitude of the shift in $\delta^{13}C$ from the initial CO reactant values to the product methane are

generally consistent with these CH_4-CO_2 equilibrium values. In this context, the scatter in the $\delta^{13}C$ values, and imperfect correlation with temperature (Figure 2a) would reflect various degrees of departure from full isotopic equilibrium and/or conversion of CO to CO_2. The FT18-4 outlier would reflect the furthest removal from CH_4-CO_2 equilibrium, and/or incomplete conversion of CO to CO_2, consistent with this experiment being conducted at the lowest temperature. The alternative interpretation is that the CH_4 $\delta^{13}C$ values reflect a kinetic carbon isotope effect involving the reduction of CO. In this case the correlation with temperature, albeit imperfect, would perhaps reflect a reservoir effect with a single kinetic fractionation factor, or a temperature-dependent kinetic fractionation factor.

5.3. The Hydrogen Isotope Balance in Our Experiments

The δD signatures of methane range from $-610‰$ to $-580‰$ V-SMOW. For experiments conducted at temperatures between 250 and 130°C, the δD of CH_4 in D/H equilibrium with water ($-119‰$ V-SMOW) would fall between $-250‰$ and $-350‰$ (Horibe & Craig, 1995). The observed δD signatures of methane are roughly $-600‰$, thus reflecting unambiguous D/H disequilibrium with water. Methane and water never reached D/H

equilibria in our catalyzed experiments. Although the presence of catalysts in our experiments would be expected to substantially accelerate D/H exchange, our data show that isotope exchange equilibrium did not occur under our experimental durations of up to 3 days. For illustration, we note that in uncatalyzed experiments, 99% D/H equilibration between methane and water takes $\sim 10^6$ days at 250°C (Turner et al., 2022).

During FTT synthesis, methane molecules form via a catalytic surface reaction of sequential hydrogen additions, presumably sourced directly from H_2 (Qi et al., 2014; Young, 2019). It is expected, therefore, that it is the D/H ratio of H_2 that is a dominant factor in controlling the D/H of methane in our experiments, not that of water. No D/H measurements of H_2 are available in this study, but at equilibrium, CH_4 should be $\sim 540‰$ higher in δD than coexisting H_2 at ~ 200°C (Horibe & Craig, 1995). In lieu of D/H for H_2 in our experiments, we may make use of three FTT experimental studies that have reported D/H of both of CH_4 and H_2 to infer the likely extent of isotopic equilibrium between these species. All of these studies report D/H ratios in CH_4 and H_2 are within 150 ‰ of each other (Fu et al., 2007; McCollom et al., 2010; Taran et al., 2010), far from the $\sim 500‰$ difference expected at equilibrium. This suggests that abiotic methane synthesized in the laboratory is not in isotopic equilibrium with H_2. We can explore this further if we assume H_2 formed in D/H equilibrium with water in our experiments. In this case δD for H_2 is predicted to be approximately $-560‰$ at 200°C, in equilibrium with the liquid water δD of $-119‰$ (Horibe & Craig, 1995; Rolston et al., 1976). According to the kinetics of $H_2O\text{-}H_2$ exchange determined experimentally (Pester et al., 2018), equilibrium should be attained in under 5 hr at 130°C and much faster at higher temperatures. This is well within experimental durations, suggesting our D/H prediction for H_2 is plausible. Since the product methane has δD values of approximately $-600‰$ at this T, it appears that the CH_4 has D/H similar to that of the reactant H_2, as in previous experiments. Under strict isotopic equilibrium between methane and an infinite pool of H_2, CH_4 should be $\sim 540‰$ higher in δD than coexisting H_2 at ~ 200°C. Similar D/H for CH_4 and H_2 therefore suggests that either the methane consumed most or all of the H_2 available locally, or, perhaps less likely, that there is a D/H kinetic fractionation that offsets the equilibrium fractionation by nearly 500‰. Overall, we conclude that a combination of equilibrium fractionation between H_2O and product H_2, followed by synthesis of methane with similar D/H to the reactant H_2 explains the methane δD values of approximately $-600‰$ obtained here.

The predicted range in δD values relative to VSMOW for H_2 formed in equilibrium with the effectively infinite reservoir of liquid H_2O from ~ 170 to 250°C is $-588‰$ to $-513‰$, respectively, defining a slope of 0.44‰/°C over this temperature range. This is similar to the observed positive correlation between methane δD values with temperature in our experiments, with a slope of $\sim 0.38‰$/°C, lending further support for the inheritance of D/H from H_2 that has equilibrated with water, with the exclusion of the 130°C outlier FT18-4 (Figure 2). This interpretation of inheritance of D/H from H_2 convolved with a kinetic isotope effect is consistent with previous similar published experiments in which the D/H values of CH_4 and H_2 are within a few tens of permil of one another (e.g., McCollom et al., 2010).

5.4. Methane Clumped Signatures: Does $^{13}CH_3D$ Reflect Peak Temperature of Methane Synthesis?

We find $\Delta^{13}CH_3D$ values to roughly track with the expected equilibrium values within 1‰ for all experiments except FT18-3 (170°C—see below), as shown in Figure 3. Data from the Sabatier experiments reported in Young et al. (2017) are also included in Figure 3. Although run under different conditions, the Sabatier experiments also show equilibrium signatures for $\Delta^{13}CH_3D$. Overall, the data suggest that FTT processes generate $\Delta^{13}CH_3D$ values that are near equilibrium at the temperature of synthesis. The equilibrium signatures suggest that despite D/H kinetic isotope effects associated with hydrogen addition during the assembly of methane molecules, the $^{13}CH_3D$ bond-ordering remains controlled by synthesis temperature. This is an important perspective for the interpretation of natural methane where abiogenesis is suspected: unless substantial mixing or degradation are involved, one may use $\Delta^{13}CH_3D$ values to constrain the approximate synthesis temperature of abiotic methane.

For FT18-3, the measured $\Delta^{13}CH_3D$ of 5.8‰ $\pm$ 0.4‰ (2 s.e.) reflects a 3‰ deviation from an equilibrium value of 2.8‰ at 170°C (Figure 3a). The equilibrium temperature corresponding to the measured $\Delta^{13}CH_3D$ value for FT18-3 is 25^{+5}_{-8}°C, far from the peak experimental temperatures, but similar to room temperature (Figure 3a). We argue against the possibility of $\Delta^{13}CH_3D$ re-equilibration toward low temperature in FT18-3 since there is no physical reason why $\Delta^{13}CH_3D$ reordering to room temperature would occur only in this experiment. Like every other experiment, gases were extracted from the gold reaction cells within 24 hr of cooling the reactors, stored in stainless steel containers, and measured for $\Delta^{13}CH_3D$ and $\Delta^{12}CH_2D_2$ at UCLA within two weeks upon synthesis.

On this basis, we argue that the elevated $\Delta^{13}CH_3D$ value for FT 18-3 must reflect an unidentified mass-dependent fractionation of up to 3‰, rather than re-equilibration.

5.5. Large $^{12}CH_2D_2$ Deficits in Abiotic Methane

The $\Delta^{12}CH_2D_2$ values here exhibit pronounced disequilibrium, in sharp contrast with those of $\Delta^{13}CH_3D$. The $\Delta^{12}CH_2D_2$ values are exclusively of negative sign, ranging from $-3.0‰ \pm 2.5‰$ (1σ) at 210°C to $-32.0‰ \pm 1.6‰$ at 183°C. These values are substantially lower than the expected equilibrium values of 9.2‰ and 4.3‰ at 130 and 250°C, respectively. We argue that the $\Delta^{12}CH_2D_2$ deficits are apparent disequilibrium signatures resulting from combinatorial effects. In general, combinatorial effects arise when a molecule contains indistinguishable atoms of the same element, and that these atoms come from pools with distinct isotope ratios, as has been predicted and for methane previously from theory (Röckmann et al., 2016; Yeung, 2016) and demonstrated for methane in the laboratory (Taenzer et al., 2020). Among the two mass-18 isotopologues of methane, only $\Delta^{12}CH_2D_2$ can be affected by combinatorial effects, because it is the isotopologue with two indistinguishable deuterium substitutions for hydrogen.

The root of the combinatorial effect comes from the notation convention used with clumped isotopes. As an example, consider a sample of methane gas with $\delta D = -100‰$ relative to SMOW and $\delta^{13}C = -10‰$ relative to PDB, corresponding to a measured bulk D/H ratio of $1.40184 \cdot 10^{-4}$ and a $^{13}C/^{12}C$ ratio of 0.01112483. In this example we will use a measured $^{12}CH_2D_2/^{12}CH_4$ ratio of 1.11600×10^{-7}. To calculate the value for $\Delta^{12}CH_2D_2$, we compute the stochastic ratio from the measured bulk carbon and hydrogen isotope ratios. Isotope-specific mole fractions for singly-substituted isotopologues are closely approximated as:

$$x_D = \frac{R_D}{1 + R_D},$$

$$x_H = \frac{1}{1 + R_D},$$

$$x_{12_C} = \frac{1}{1 + R_{13_C}}, \tag{5}$$

where R_D is the bulk D/H ratio and R_{13C} is the bulk $^{13}C/^{12}C$ ratio. From the properties of probabilities, the stochastic isotope-specific mole fraction of $^{12}CH_2D_2$, where isotopes are distributed randomly across all isotopologues, is:

$$x_{12_{CH_2D_2}} = 6x_D^2 x_H^2 x_{12_C}, \tag{6}$$

where 6 refers to the six isotopic isomers for this isotopologue ($^{12}CHDHD$, $^{12}CHHDD$, $^{12}CDHDH$, etc.). In this example, the stochastic value for $x^{12}CH_2D_2$ is 1.16547×10^{-7} and the stochastic value for $x^{12}CH_4 = xH^4 \, x^{12}C$ is 0.9884432. With a measured $^{12}CH_2D_2/^{12}CH_4$ ratio of 1.16000×10^{-7}, we have:

$$\Delta CH_2D_2 = 10^3 \left(\frac{\frac{(12_{CH_2D_2})}{(12_{CH_4})_{measured}}}{\frac{(12_{CH_2D_2})}{(12_{CH_4})_{stochastic}}} - 1 \right) = -16.2‰ \tag{7}$$

Now let us consider the possibility that in the same gas, the methane molecules were in fact constructed from two pools of hydrogen with distinct D/H ratios, with the average D/H being the measured bulk value in our methane, that is, $\delta D = -100‰$. If α is the fractionation factor relating the D/H ratios for the two pools, then:

$$\frac{(R_1 + \alpha R_1)}{2} = R_D \tag{8}$$

where R_1 is the D/H for one of the reservoirs, $\alpha R_1 = R_2$ is the D/H for the other reservoir, and R_D is the measured bulk ratio. For illustration, we take $\alpha = 1.5$, meaning two hydrogens have a D/H ratio fractionated by +500‰ relative to the two other hydrogens. Now the true stochastic ratio, given a priori knowledge of equal contributions
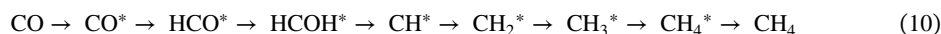
from the two pools, is given by the corresponding mole fractions for the two pools, $x_{D(1)}$, $x_{D(2)}$ etc., so Equation 6 becomes:

$$x_{12_{CH_2D_2}} = 6x_{D(1)}x_{D(2)}x_{H(1)}x_{H(2)}x_{12_C}. \tag{9}$$

Similarly, the stochastic mole fraction for $^{12}CH_4$ is $x^{12}CH_4 = xH_{(1)}^2 \, xH_{(2)}^2 \times \, ^{12}C$. In our example, the true stochastic value for $x^{12}CH_2D_2$ is 1.11885×10^{-7}. This is lower by 42‰ than 1.16545×10^{-7}, the value obtained from Equation 6. Using the stochastic estimate from Equation 9, the example gas has a true $\Delta^{12}CH_2D_2$ of +25‰.

In practice, one would not have any prior knowledge of the actual distribution of the D/H ratios and would have to apply Equation 6 rather than Equation 9 for the calculation of $\Delta^{12}CH_2D_2$. The elevated $x^{12}CH_2D_2$ from Equation 6 is the cause of the negative $\Delta^{12}CH_2D_2$ value. The reason for the discrepancy is a mathematical truism (Rockmann et al., 2016; Taenzer et al., 2020; Yeung, 2016). It is straightforward to show that the actual stochastic isotopologue ratio $^{12}CH_2D_2/^{12}CH_4$ is proportional to the square of the geometric mean for the two D/H ratios (to see this, divide Equation 9 by $x^{12}CH_4 = xH_{(1)}^2 \, xH_{(2)}^2 \, x^{12}C$) while the measured values, by necessity, yield the square of the arithmetic mean of the two ratios, that is, the measured bulk D/H ratio (divide Equation 6 by $x^{12}CH_4 = xH_4 \, x^{12}C$, mindful of Equation 8). The geometric mean is always less than the arithmetic mean, unless $R_1 = R_2$. Thus in general, where molecular positions with distinct isotope ratios are indistinguishable, and the average isotope ratios rather than the site-specific isotope ratios are all that is accessible by the data (the usual case), the calculated stochastic ratio of the multiply-substituted molecule to the major isotopologue ($x^{12}CH_2D_2$) is overestimated. This in turn means Δ values derived from these overestimated stochastic ratios are underestimated. This is the combinatorial effect.

The building of CH_4 molecules from CO (or CO_2) is thought to involve a sequence of steps of carbon reduction followed by additions of hydrogen molecules (Qi et al., 2014; W. Wang et al., 2011; Young, 2019; Young et al., 2017). The set of reactions for the assembly of methane may be represented by these steps:

$$CO \rightarrow CO^* \rightarrow HCO^* \rightarrow HCOH^* \rightarrow CH^* \rightarrow CH_2{}^* \rightarrow CH_3{}^* \rightarrow CH_4{}^* \rightarrow CH_4 \tag{10}$$

where * corresponds to a surface-adsorbed species. Here, H_2 is the source of electrons for reduction. This reaction network allows for the various hydrogens added to methane during sequential steps to have different D/H ratios. This reflects an "endogenous" combinatorial effect, resulting strictly from D/H fractionations associated with the assembly of methane molecules from one pool of hydrogen. This is different from an "exogenous" combinatorial effect, where D/H variations are inherited from multiple sources of H_2.

A 500‰ difference between two of the hydrogens relative to the other two can account for our observed $\Delta^{12}CH_2D_2$ deficits of approximately −40‰. The particular circumstance of $\delta D_{(1)} = \delta D_{(2)} = -850‰$ and $\delta D_{(3)} = \delta D_{(4)} = -350‰$ can explain the bulk methane δD (∼−600‰), and the methane clumped isotope values. According to the theoretical treatments in Cao et al. (2019) and Young (2019), D/H fractionations associated with the assembly of methane would plausibly cause such variations in D/H from step to step. For example, a mixture of early steps involving D/H equilibrium followed by later H addition steps with purely kinetic isotope effects could produce the requisite large differences in D/H of >400‰ among hydrogens (Young, 2019) that can reproduce the observed low $\Delta^{12}CH_2D_2$ values.

The question arises as to whether our interpretation of the source of low $\Delta^{12}CH_2D_2$ values is affected by the source of carbon, that is, CO versus CO_2. CO_2 methanation begins by reduction to CO (i.e., the reverse of reaction 4) represented as an additional step on Figure 4. That additional step occurs prior to the onset of CO reduction and does not involve hydrogen additions to carbon. There is no clear physical reason to anticipate variable $\Delta^{12}CH_2D_2$ signatures as the result of the additional step of CO_2 reduction to CO prior to further reduction by hydrogen. This likely explains why the Sabatier experiments (run with CO_2) versus the FTT experiments here (with CO) can be interpreted together (Figure 3b). Indeed, our data suggests the two pathways, from CO to methane and from CO_2 to methane, may not be very different at all with respect to their isotopic effects. Our carbon isotope data suggesting that CO_2 is the precursor for the $^{13}C/^{12}C$ ratios for product CH_4 in our experiments in which CO is the initial carrier of carbon attest to this. Together, the data indicate that it may be valid to extrapolate our experiments to natural systems, where CO_2 is likely the ultimate primary carbon source for abiotic methane synthesis.
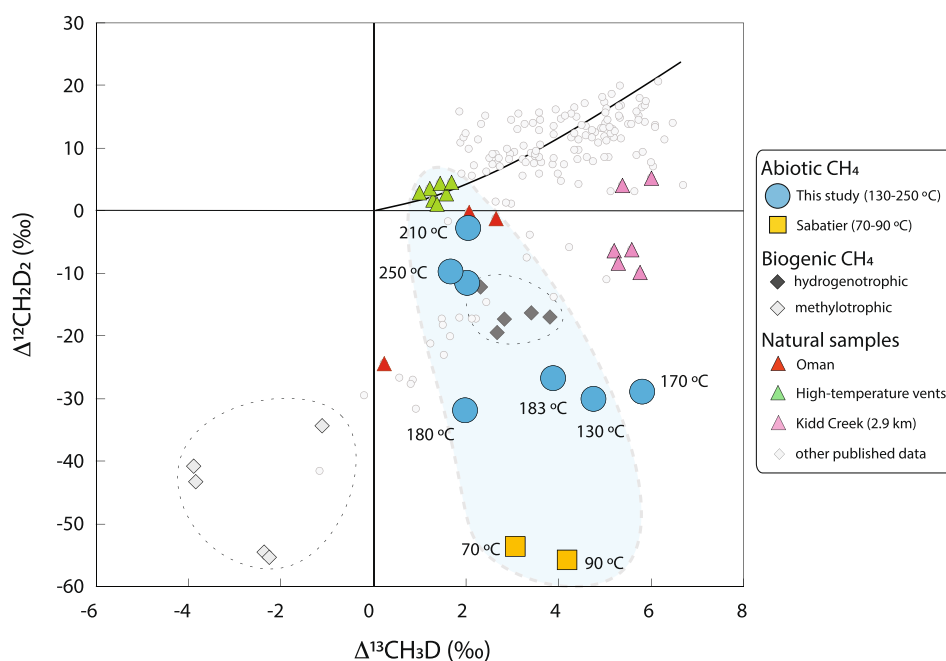
Figure 4. The two mass-18 isotopologues of methane for relevant experimental and natural data. The Fischer-Tropsch-Type data are from this work. A tentative abiotic field is drawn in light blue. The Sabatier experiments are from Young et al. (2017). Microbial methane data are from Young et al. (2017) and Giunta et al. (2019). Fields are drawn around the hydrogenotrophic and methylotrophic pathways. Hydrothermal gases are from the Rainbow, Von Damm, and Lucky Strike sites from Labidi et al. (2020). The Kidd Creek data are only from the 2.9 km level in the mine, from Young et al. (2017). The Oman data are from various vents in the ophiolite, and the data can be found in Nothaft et al. (2021). Open symbols are natural data from various geological settings are from Ash et al. (2018), Giunta et al. (2019, 2021), Gonzalez et al. (2019), Lin et al. (2023), Warr et al. (2021), Young et al. (2017), and Young (2019).

5.6. The Temperature Relationship With $\Delta^{12}CH_2D_2$

Experiments with data at the highest temperatures, 210 and 250°C, produced methane with $\Delta^{12}CH_2D_2$ values of between −3‰ and −12‰. This is substantially more positive than in experiments done at 180, 170, and 130°C, which produced methane with $\Delta^{12}CH_2D_2$ values of between −32‰ and −27‰ (Figure 3b). The Sabatier experiments at $T \leq 90°C$ (Young et al., 2017) yielded methane with $\Delta^{12}CH_2D_2$ values of roughly −55‰. Taken together, the $\Delta^{12}CH_2D_2$ data show a clear positive correlation with temperature (Figure 3b). This may reflect the possibility that different D/H ratios among pools of hydrogen at each reaction step are dependent on temperature, with greater differences at lower temperatures. At >200°C, the observed $\Delta^{12}CH_2D_2$ values require pools of hydrogen atoms that comprise methane to be at most 200 ‰ different from one another. At <100°C, the 70‰ $\Delta^{12}CH_2D_2$ deficits of the Sabatier experiments require at least 700‰ D/H difference between pools of hydrogen atoms.

The effect of bond reordering is unclear in this set of experiments. One might imagine that irrespective of experimental temperatures, all abiotic methane synthesized during FTT experiments is associated with $\Delta^{12}CH_2D_2$ deficits >70‰, as the natural consequence of extreme and variable D/H fractionation factors among the four hydrogen addition steps. This would be the case if kinetic isotope effects for each step in the CH$_4$-building reaction sequence were fully independent of temperature. After methane synthesis, $\Delta^{12}CH_2D_2$ values would approach equilibrium values > 0‰ due to bond reordering. Bond reordering—here, homogenization of the D/H among the hydrogens comprising CH$_4$ molecules—would generate an *a-posteriori* correlation between temperature and $\Delta^{12}CH_2D_2$ as observed on Figure 3b. This scenario may not be excluded. Nonetheless, we favor a temperature-dependent fractionation in D/H between H-addition steps during CH$_4$ construction as the source of negative $\Delta^{12}CH_2D_2$ values since these effects can be seen in the theoretical treatments in Cao et al. (2019) and Young (2019).

To summarize, the $\Delta^{12}CH_2D_2$ relationship with experimental temperature (Figure 3b) may be explained by two different scenarios. First, kinetic isotope effects for different H-addition steps may vary as a function of temperature. This would cause the resulting combinatorial $\Delta^{12}CH_2D_2$ values to show a variability naturally correlated to temperature. Alternatively, an a-posteriori bond reordering may occur in the hydrothermal reaction vessel, from an initial $\Delta^{12}CH_2D_2$ value that is always $-70‰$. If experiments at higher temperature allow further re-ordering than those at lower temperatures, temperature and $\Delta^{12}CH_2D_2$ will display a positively correlation.

5.7. Distinguishing Biogenic From Abiotic Sources of Methane

The data collected for this study are plotted on Figure 4 with published methane isotopologue data for biogenic methane synthesized in the laboratory, and for natural samples from a variety of geological settings, including sedimentary basins, deep crystalline environments and serpentinization sites (Ash et al., 2018; Giunta et al., 2019, 2021; Lin et al., 2023; Young, 2019; Young et al., 2017; Warr et al., 2021). Extreme signatures associated with anaerobic oxidation of methane (Giunta et al., 2022; Liu et al., 2023) were omitted for clarity. Signatures observed in abiotic methane are unique in their magnitude of $\Delta^{12}CH_2D_2$ deficits at elevated $\Delta^{13}CH_3D$. Such signatures are rare in nature (Figure 4), potentially suggesting that abiotic methane has been under-sampled so far.

Microbial methane shows $\Delta^{12}CH_2D_2$ deficits (Giunta et al., 2019; Young et al., 2017), and thus could potentially be confused with abiotic CH_4. Biogenic CH_4 synthesized via the methylotrophic pathways at 30–37°C exhibits $\Delta^{12}CH_2D_2$ deficits associated with largely negative $\Delta^{13}CH_3D$ values (Young et al., 2017). This is clearly different from the signatures of abiotic methane reported here. Acetoclastic methane has been characterized for its $\Delta^{13}CH_3D$ signatures only. Disequilibrium negative values were found (Gruen et al., 2018), suggesting a potential proximity to the methylotrophic field in clumping space. The negative $\Delta^{13}CH_3D$ are probably the result of classical kinetics involving carbon isotopes (Giunta et al., 2019; Gruen et al., 2018; Young et al., 2017). Anomalously low $\Delta^{13}CH_3D$ represent an opportunity to distinguish methylotrophic microbial CH_4 from any other source of methane, assuming no degradation or mixing occurred. This is important where there is a demand to constrain abiotic contributions for natural settings where methylotrophic (or acetoclastic) synthesis is also suspected to occur, or has been hypothetically considered such as Enceladus (see below). Methane synthesized via the hydrogenotrophic pathway at temperatures between 37 and 65°C has $\Delta^{13}CH_3D$ of $\sim+3‰$ and $\Delta^{12}CH_2D_2$ of $\sim-20‰$. These signatures are different from the other pathways and resemble the abiotic signatures generated at 250°C, with $\Delta^{13}CH_3D$ of $\sim+2‰$ and $\Delta^{12}CH_2D_2$ of $\sim-10‰$ (Figure 4). This means that in the restrictive case of abiotic methane synthesized at the right temperature, it may not be distinguished from biogenic methane synthesized via the hydrogenotrophic pathway.

There might be a need to distinguish thermogenic from abiotic CH_4 in specific settings (Shuai et al., 2018). Variable $\Delta^{12}CH_2D_2$ deficits associated with positive $\Delta^{13}CH_3D$ values have been reported for thermogenic CH_4 of very low maturity in nature (Xie et al., 2021) and in the laboratory (Dong et al., 2021). The signatures observed in natural samples resembles abiotic methane generated at $\sim250°C$ (and microbial CH_4 from the hydrogenotrophic pathway) so identification would be challenging. However, in most cases, thermogenic methane typically shows near-equilibrium $\Delta^{12}CH_2D_2$ and $\Delta^{13}CH_3D$ values, at temperatures relevant to basins (Dong et al., 2021; Giunta et al., 2019, 2021; Lin et al., 2023; Xie et al., 2021; Young et al., 2017). This is distinct from what we observe and suggests that in most settings, the $\Delta^{12}CH_2D_2$-$\Delta^{13}CH_3D$ signatures of thermogenic methane may not be confused with those of abiotic CH_4.

Overall, methane clumping is helpful to unambiguously distinguish abiotic methane from microbial methane, from both methylotrophic and acetotrophic pathways in nature. For microbial methane from the hydrogenotrophic pathway, and for the specific case of immature thermogenic CH_4, distinction from abiotic sources is more challenging on the basis of $\Delta^{12}CH_2D_2$-$\Delta^{13}CH_3D$ data alone. We note however that methane generated abiotically at temperatures below 200°C would show $\Delta^{12}CH_2D_2$ values below $-30‰$, at $\Delta^{13}CH_3D > 2‰$. The $\Delta^{12}CH_2D_2$ deficits are much deeper than what is observed with hydrogenotrophic microbial methane and immature thermogenic methane in nature, allowing clear identification. We suggest that those signatures could therefore be used as tracers for abiogenesis on Earth and on other worlds.

5.8. Bond Re-Ordering in Nature: The Link With the Laboratory

Based on experiments, we would anticipate natural abiotic methane synthesized in high-temperature hydrothermal vents with temperatures $\geq250°C$ to have equilibrated $\Delta^{13}CH_3D$ values associated with $\sim10‰$ $\Delta^{12}CH_2D_2$

deficits relative to equilibrium (Figure 3b). Instead, equilibrium values for $\Delta^{12}CH_2D_2$ (and $\Delta^{13}CH_3D$) are seen in most samples, to date (Figure 4). Subsequent bond reordering would seem to be required in order to erase the low $\Delta^{12}CH_2D_2$ values associated with constructing CH_4 molecules and replace them with the equilibrium values exhibited by the natural high-temperature hydrothermal samples. High-temperature hydrothermal systems may provide conditions conducive to bond reordering. Methane is thought to be formed abiotically in fluid inclusions of basement rocks at temperatures of 300°C or higher (Früh-Green et al., 2022; Klein et al., 2019). Those fluid inclusions might be maintained at temperatures of 300°C or above for durations that may be thousands of years or even far longer, allowing bond reordering to take place. At Lost City, $\Delta^{12}CH_2D_2$ have been modified even further. There, fluids containing methane are vented at temperatures under 96°C (Kelley et al., 2005). D/H and $\Delta^{13}CH_3D$ data indicate equilibration at ~250°C (D. T. Wang et al., 2018). This means that methane was brought to 250°C, perhaps during synthesis, and subsequently cooled down to venting temperatures. The cooling of hydrothermal fluids was evidently too rapid to cause major D/H shifts or $\Delta^{13}CH_3D$ re-ordering (Labidi et al., 2020; D. T. Wang et al., 2018). In contrast, $\Delta^{12}CH_2D_2$ values are re-ordered to higher values, consistent with equilibrium at venting temperature (Labidi et al., 2020). The data require fluid cooling at Lost City at rates that allow near-complete $\Delta^{12}CH_2D_2$ re-ordering to equilibrium with venting temperatures but precluding reordering of $\Delta^{13}CH_3D$, appearing as $\Delta^{12}CH_2D_2$ excesses at a given $\Delta^{13}CH_3D$ (Labidi et al., 2020). Taken together, observations suggest that in natural hydrothermal systems, where methane is initially formed at high temperature, the $\Delta^{12}CH_2D_2$ deficits associated with initial methane synthesis are "cryptic," that is, they tend to be replaced with equilibrium signatures or apparent excesses.

Abiotic methane formed and kept at low temperature might have a chance to preserve deficits in $\Delta^{12}CH_2D_2$, should it be restricted to environments where the kinetics of D/H homogenization within methane molecules are unfavorable or residence times are short. This offers a chance to use the combination of $\Delta^{12}CH_2D_2$ and $\Delta^{13}CH_3D$ to identify abiotic methane in nature, as it has been done with microbial methane (Ash et al., 2018; Giunta et al., 2019, 2022; Young et al., 2017). Abiogenesis may notably account for signatures observed in methane from ~25°C fluids from the Kidd Creek mine. There, methane samples have $\Delta^{13}CH_3D$ values of 5.2‰ ± 0.5‰, translating to temperatures of ~45°C. The methane $\Delta^{12}CH_2D_2$ values from the deepest level in the mine are 10‰–30‰ below equilibrium (data in Young et al., 2017, also shown here on Figure 4). These deficits are not as low as those seen in experiments, and would be compatible with FTT signatures affected by later bond reordering resulting from processing by anaerobic methane oxidation (Warr et al., 2021; Young et al., 2017).

Abiogenesis alone is more challenging to reconcile with the observations from serpentinizing systems in Oman. There, methane is vented to the surface in ~35°C hyperalkaline fluids issuing from the underlying ophiolite. It carries some of the highest $\delta^{13}C$ yet measured in natural methane (Miller et al., 2016). Whether microbial methanogenesis can explain the isotopic features of Oman methane is debated (Etiope, 2017; Miller et al., 2016). Recent measurements of $\Delta^{12}CH_2D_2$ and $\Delta^{13}CH_3D$ were made available on new gas aliquots from Oman, in Nothaft et al. (2021). The one sample with the highest $\delta^{13}C$ has a negative $\Delta^{12}CH_2D_2$ value and near-zero $\Delta^{13}CH_3D$ (Figure 4). This is inconsistent with abiotic signatures reported here: no abiotic methane made in the laboratory, at any of the investigated temperatures, has yielded a near-zero $\Delta^{13}CH_3D$ (Figure 3a). Conversely, microbial methane does exhibit near-zero or negative $\Delta^{13}CH_3D$ values, especially microbial methane synthesized via the methylotrophic pathways (Giunta et al., 2019; Young et al., 2017). The simplest explanation for the data in Nothaft et al. (2021) remains that despite the elevated $\delta^{13}C$, the $\Delta^{12}CH_2D_2$-$\Delta^{13}CH_3D$ signature reflect substantial contributions of microbial methane in the Oman ophiolite (details in Nothaft et al., 2021).

5.9. Methane Clumped Signatures in Astrobiology

Methane has been detected in Mars's atmosphere (Formisano et al., 2004; Krasnopolsky et al., 2004; Mumma et al., 2009; Webster et al., 2015) and rocks (Blamey et al., 2015; House et al., 2022), indicating that methane is produced in the subsurface of the planet. Methane has been observed in Enceladus' geysers (Waite et al., 2006). It is the second most abundant species in Titan's N_2-dominated atmosphere (Niemann et al., 2005; Tyler et al., 1981). It is also detected on the surface of icy bodies present in the trans-Neptunian region of the solar system. This includes Triton, Pluto and Charon (Cruikshank et al., 1998; Grundy et al., 2016; Owen et al., 1993), and of at least two dwarf planets with trans-Neptunian orbits (Glein et al., 2024; Grundy et al., 2024). In addition, methane has been recently observed in the atmosphere of the gaseous giant exoplanet WASP-80b atmosphere (Bell et al., 2023). The origin of methane on these bodies is unclear. Observations of methane on terrestrial planets and icy bodies might reflect ancient or modern hydrothermal activity which led to the synthesis of abiotic methane

(Glein, 2015; Mumma et al., 2009). Alternatively, microbial contributions are being considered (Affholder et al., 2021; Atreya et al., 2007).

It is not clear that conventional isotopic tools alone can yield unambiguous results as to the origin of methane on other planets, because sound interpretations of bulk isotope ratios by conventional means require contextual information: what is the meaning of methane D/H ratios with no constraints on the D/H of the co-existing molecular hydrogen? What is the overall $^{13}C/^{12}C$ of the carbon reservoirs from which methane might evolve? This is underscored by the complex interpretations of $^{13}C/^{12}C$ ratios measured on Mars rocks by Curiosity (House et al., 2022). In contrast, mass-18 isotopologues of methane may be a useful tool. Our experiments suggest methane produced by abiogenesis on other worlds may have tell-tale $\Delta^{12}CH_2D_2$ deficits. This is because the difference between Equations 6 and 9 remains insensitive to the absolute value of the D/H ratio; only D/H *differences* between various hydrogen pools matter in causing combinatorial effects (Rockmann et al., 2016; Taenzer et al., 2020), not the absolute values of the source pools. Since D/H differences inevitably follow from lower-T hydrogen additions to carbon, we expect $\Delta^{12}CH_2D_2$ deficits to be common anywhere methane is synthesized from the reduction of CO or CO_2. This means that on other worlds, where the D/H ratio of molecular hydrogen is unknown and could be extremely different from Earth, abiotic methane should still exhibit $\Delta^{12}CH_2D_2$ deficits comparable to the values observed here (Figure 3).

Methane present on the surface of Pluto and other icy bodies is thought to have been emitted from the interior of the planetesimals by cryovolcanic degassing (Glein et al., 2024; Moore & McKinnon, 2021). These planetary surfaces are, however, exposed to irradiation by cosmic and sun rays, which likely partially destroys CH_4 (Hudson et al., 2008). Atmospheric photodissociation of methane occurs on Titan (Strobel, 1974), which also leads to the partial obliteration of the pristine CH_4 budget of the planetary surface. This would almost certainly destroy the $\Delta^{13}CH_3D-\Delta^{12}CH_2D_2$ signatures of the sources of CH_4. For this reason, applications of methane clumping on Mars and Enceladus may be more promising.

The in-situ discovery of methane gas in Mars's atmosphere by Curiosity (Webster et al., 2015) indicates that methane is produced on the planet, likely from an on-going source in the subsurface. The source of methane on Mars has been suggested to be both biogenic or abiotic (Atreya et al., 2007; Mumma et al., 2009). We suggest that $\Delta^{13}CH_3D-\Delta^{12}CH_2D_2$ signatures would clearly differentiate abiotic from biogenic methane if methylotrophic and acetoclastic pathways had been dominant in generating methane at any point in Mars's history. This has been recently considered unlikely, and hydrogenotrophic methanogenesis was flagged as the potential dominant pathway for microbial methane synthesis on Early Mars (Sauterey et al., 2022). Should abiotic methane on Mars be synthesized at temperatures between 200 and 250°C, it would exhibit $\Delta^{13}CH_3D-\Delta^{12}CH_2D_2$ signatures indistinguishable from biogenic methane (Figure 4). If so, $\Delta^{13}CH_3D-\Delta^{12}CH_2D_2$ data would not differentiate between Martian methane being abiotic or biogenic. Conversely, for abiotic methane synthesized at any temperatures under 200°C on Mars, it would be unambiguously identified via the display of deep $\Delta^{12}CH_2D_2$ deficits at a given $\Delta^{13}CH_3D$, as observed with our experiments.

Molecular hydrogen and methane were found together in the geysers of Enceladus (Waite et al., 2017). The plumes H_2/CH_4 ratios are ~1–14, consistent with modern hydrothermal activity and/or microbial activity occurring in Enceladus's ocean (Waite et al., 2017). Like on Mars, biogenic methane synthesized via the hydrogenotrophic pathway could be confused with abiotic methane formed at temperatures between 200 and 250°C. However, among the microbial pathways, the acetoclastic metabolism could be best fit to dominate the production of biogenic methane on Enceladus, if microbial methanogenesis is present at all. This is because the presence of acetylene on Enceladus would favor microbial acetylenotrophy (Yanez et al., 2024), a by-product of which is acetate. A scenario where acetylenotrophy occurs on Enceladus would therefore allow the accumulation of acetate in Enceladus' internal ocean, thus providing the substrate for acetoclastic methanogenesis. Acetoclastic methane has negative $\Delta^{13}CH_3D$ values (Gruen et al., 2018). This is different from the exclusively positive $\Delta^{13}CH_3D$ values observed here for abiotic methane. We tentatively conclude that $\Delta^{13}CH_3D-\Delta^{12}CH_2D_2$ measurements on methane from Enceladus plumes would differentiate abiotic from biogenic methane synthesized by the acetoclastic pathway, without having to know the D/H of H_2 or the $^{13}C/^{12}C$ of the carbon source. Should methane be abiotic, $\Delta^{13}CH_3D$ data would show clearly positive values as observed in our experiments. The $\Delta^{13}CH_3D$ values would thus provide important constraints on the temperature of abiotic methane formation, following the temperature relationship observed on Figure 3a.

An important caveat to this conclusion is the potential for bond re-ordering that would erase the isotopologue signatures of methane formation pathways. If methane was circulated in a hydrothermal system with ambient temperatures approaching 300°C, $\Delta^{13}CH_3D$-$\Delta^{12}CH_2D_2$ signatures associated with methane synthesis might have been replaced by isotopologue equilibrium, as is observed in at least some hydrothermal systems on Earth (Labidi et al., 2020). The simplest explanation for $\Delta^{13}CH_3D$-$\Delta^{12}CH_2D_2$ signatures of equilibration at high temperature on alien worlds is that the conditions prevalent in hydrothermal systems allowed both reaction 1 to occur abiotically and, with time, forced the abiotic methane to reorder $\Delta^{13}CH_3D$-$\Delta^{12}CH_2D_2$ values. Bond re-ordering could be a silver lining in the identification of abiosignatures: In addition to offering an indirect observation for a high-temperature hydrothermal circulation, the relatively high-T equilibrium $\Delta^{13}CH_3D$-$\Delta^{12}CH_2D_2$ values would be a unique signature that cannot be generated by microbial activity. The isotopic observation of high-temperature equilibria could be considered an indirect abiosignature, and would constitute robust evidence for high-temperature hydrothermal circulations on other worlds.

6. Conclusion

We performed synthesis of abiogenic methane in the laboratory and determined $\delta^{13}C$, δD, $\Delta^{13}CH_3D$, and $\Delta^{12}CH_2D_2$ using a Panorama gas-source mass spectrometer. We carried out a set of 9 experiments in hydrothermal conditions, at temperatures between 130 and 300°C. The experiments were performed by heating an aqueous solution in the presence of Fe^0 powder and gaseous CO. We find $\delta^{13}C$ and δD of methane to be isotopically depleted relative to the starting materials, consistent with equilibrium carbon isotope fractionation between CO_2 produced in the experiment and the product CH_4, and kinetic isotope D/H fractionations between H_2 and product CH_4. We find most of the product methane $\Delta^{13}CH_3D$ values trace the temperature of abiotic methane synthesis within a permil. At the same time, we observe $\Delta^{12}CH_2D_2$ deficits of up to 40‰ relative to equilibrium attributable to a D/H combinatorial effect occurring during the methane assembly. The combinatorial effect results from our inability to determine D/H ratios of distinctive pools of hydrogen that contribute to individual hydrogens on the methane molecule. The D/H fractionation associated with the various steps of hydrogen addition to carbon can explain the direction and the magnitude of the $\Delta^{12}CH_2D_2$ signatures of methane that would otherwise be at bond-ordering equilibrium. In instances of some potentially abiotic methane found on Earth, particularly under high T, $\Delta^{12}CH_2D_2$ deficits may have been generated during methane synthesis, but were subsequently erased by D/H reordering. In contrast, $\Delta^{12}CH_2D_2$ deficits generated in our experiments are seen on Earth at sites where the C-H bond activation was too slow to re-equilibrate $\Delta^{12}CH_2D_2$ values to environmental temperatures. As such these dramatic deficits, when combined with near-equilibrium $\Delta^{13}CH_3D$ values, might be an avenue for the identification of abiogenesis on other worlds.

Data Availability Statement

All the methane isotope data collected for this study are available online via the EarthChem data repository, and referenced here as Labidi et al. (2024).

References

Affholder, A., Guyot, F., Sauterey, B., Ferrière, R., & Mazevet, S. (2021). Bayesian analysis of Enceladus's plume data to assess methanogenesis. *Nature Astronomy*, 5(8), 805–814. https://doi.org/10.1038/s41550-021-01372-6

Ash, J. L., Egger, M., Treude, T., Kohl, I., Cragg, B., Parkes, R. J., et al. (2018). Exchange catalysis during anaerobic methanotrophy revealed by $^{12}CH_2D_2$ & $^{13}CH_3D$ in methane. In *bioRxiv 377531*.

Atreya, S. K., Mahaffy, P. R., & Wong, A.-S. (2007). Methane and related trace species on Mars: Origin, loss, implications for life, and habitability. *Planetary and Space Science*, 55(3), 358–369. https://doi.org/10.1016/j.pss.2006.02.005

Bell, T. J., Welbanks, L., Schlawin, E., Line, M. R., Fortney, J. J., Greene, T. P., et al. (2023). Methane throughout the atmosphere of the warm exoplanet WASP-80b. *Nature*, 623(7988), 709–712. https://doi.org/10.1038/s41586-023-06687-0

Berndt, M. E., Allen, D. E., & Seyfried, W. E. (1996). Reduction of CO_2 during serpentinization of olivine at 300°C and 500 bar. *Geology*, 24(4), 351–354. https://doi.org/10.1130/0091-7613(1996)024<0351:rocdso>2.3.co;2

Blamey, N. J. F., Parnell, J., McMahon, S., Mark, D. F., Tomkinson, T., Lee, M., et al. (2015). Evidence for methane in Martian meteorites. *Nature Communications*, 6(1), 7399. https://doi.org/10.1038/ncomms8399

Bradley, A. S., & Summons, R. E. (2010). Multiple origins of methane at the lost City hydrothermal field. *Earth and Planetary Science Letters*, 297(1–2), 34–41. https://doi.org/10.1016/j.epsl.2010.05.034

Cao, X., Bao, H., & Peng, Y. (2019). A kinetic model for isotopologue signatures of methane generated by biotic and abiotic CO_2 methanation. *Geochimica et Cosmochimica Acta*, 249, 59–75. https://doi.org/10.1016/j.gca.2019.01.021

Charlou, J. L., Donval, J. P., Konn, C., OndréAs, H., Fouquet, Y., Jean-Baptiste, P., & Fourré, E. (2010). High production and fluxes of H_2 and CH_4 and evidence of abiotic hydrocarbon synthesis by serpentinization in ultramafic-hosted hydrothermal systems on the Mid-Atlantic Ridge. Divers. *Geophysical Monograph Series*, *188*, 265–296.

Cruikshank, D. P., Roush, T. L., Owen, T. C., Quirico, E., & Bergh, C. D. (1998). The surface compositions of Triton, Pluto, and Charon. In *Solar system Ices: Based on reviews presented at the international symposium "solar system ices" held in Toulouse, France, on March 27–30, 1995* (pp. 655–684). Springer.

Dong, G., Xie, H., Formolo, M., Lawson, M., Sessions, A., & Eiler, J. (2021). Clumped isotope effects of thermogenic methane formation: Insights from pyrolysis of hydrocarbons. *Geochimica et Cosmochimica Acta*, *303*, 159–183. https://doi.org/10.1016/j.gca.2021.03.009

Douglas, P. M. J., Stolper, D. A., Eiler, J. M., Sessions, A. L., Lawson, M., Shuai, Y., et al. (2017). Methane clumped isotopes: Progress and potential for a new isotopic tracer. *Organic Geochemistry*, *113*, 262–282. https://doi.org/10.1016/j.orggeochem.2017.07.016

Etiope, G. (2017). Methane origin in the Samail ophiolite: Comment on "modern water/rock reactions in Oman hyperalkaline peridotite aquifers and implications for microbial habitability. *Geochimica et Cosmochimica Acta*, *179*(2016), 217–241.

Etiope, G., & Ionescu, A. (2015). Low-temperature catalytic CO_2 hydrogenation with geological quantities of ruthenium: A possible abiotic CH_4 source in chromitite-rich serpentinized rocks. *Geofluids*, *15*(3), 438–452. https://doi.org/10.1111/gfl.12106

Etiope, G., Judas, J., & Whiticar, M. J. (2015). Occurrence of abiotic methane in the eastern United Arab Emirates ophiolite aquifer. *Arabian Journal of Geosciences*, *8*(12), 11345–11348. https://doi.org/10.1007/s12517-015-1975-4

Etiope, G., & Sherwood Lollar, B. (2013). Abiotic methane on Earth. *Reviews of Geophysics*, *51*(2), 276–299. https://doi.org/10.1002/rog.20011

Etiope, G., & Whiticar, M. J. (2019). Abiotic methane in continental ultramafic rock systems: Towards a genetic model. *Applied Geochemistry*, *102*, 139–152. https://doi.org/10.1016/j.apgeochem.2019.01.012

Fenchel, T., Blackburn, H., & King, G. M. (2012). *Bacterial biogeochemistry: The ecophysiology of mineral cycling*. Academic Press.

Formisano, V., Atreya, S., Encrenaz, T., Ignatiev, N., & Giuranna, M. (2004). Detection of methane in the atmosphere of Mars. *Science*, *306*(5702), 1758–1761. https://doi.org/10.1126/science.1101732

Foustoukos, D. I., & Seyfried, W. E., Jr. (2004). Hydrocarbons in hydrothermal vent fluids: The role of Chromium-bearing catalysts. *Science*, *304*(5673), 1002–1005. https://doi.org/10.1126/science.1096033

Fritz, P., Clark, I. D., Fontes, J.-C., Whiticar, M. J., & Faber, E. (1992). Deuterium and 13C evidence for low temperature production of hydrogen and methane in a highly alkaline groundwater environment in Oman. *Proceedings International Symposium on Water-Rock Interaction*, *7*, 793–796.

Früh-Green, G. L., Kelley, D. S., Lilley, M. D., Cannat, M., Chavagnac, V., & Baross, J. A. (2022). Diversity of magmatism, hydrothermal processes and microbial interactions at mid-ocean ridges. *Nature Reviews Earth & Environment*, *3*(12), 1–20. https://doi.org/10.1038/s43017-022-00364-y

Fu, Q., Sherwood Lollar, B., Horita, J., Lacrampe-Couloume, G., & Seyfried, J. W. E. (2007). Abiotic formation of hydrocarbons under hydrothermal conditions: Constraints from chemical and isotope data. *Geochimica et Cosmochimica Acta*, *71*(8), 1982–1998. https://doi.org/10.1016/j.gca.2007.01.022

Giunta, T., Labidi, J., Kohl, I. E., Ruffine, L., Donval, J. P., Géli, L., et al. (2021). Evidence for methane isotopic bond re-ordering in gas reservoirs sourcing cold seeps from the Sea of Marmara. *Earth and Planetary Science Letters*, *553*, 116619. https://doi.org/10.1016/j.epsl.2020.116619

Giunta, T., Young, E. D., Labidi, J., Sansjofre, P., Jézéquel, D., Donval, J.-P., et al. (2022). Extreme methane clumped isotopologue bio-signatures of aerobic and anaerobic methanotrophy: Insights from the Lake Pavin and the Black Sea sediments. *Geochimica et Cosmochimica Acta*, *338*, 34–53. https://doi.org/10.1016/j.gca.2022.09.034

Giunta, T., Young, E. D., Warr, O., Kohl, I., Ash, J. L., Martini, A., et al. (2019). Methane sources and sinks in continental sedimentary systems: New insights from paired clumped isotopologues $^{13}CH_3D$ and $^{12}CH_2D_2$. *Geochimica et Cosmochimica Acta*, *245*, 327–351. https://doi.org/10.1016/j.gca.2018.10.030

Glein, C. R. (2015). Noble gases, nitrogen, and methane from the deep interior to the atmosphere of Titan. *Icarus*, *250*, 570–586. https://doi.org/10.1016/j.icarus.2015.01.001

Glein, C. R., Grundy, W. M., Lunine, J. I., Wong, I., Protopapa, S., Pinilla-Alonso, N., et al. (2024). Moderate D/H ratios in methane ice on Eris and Makemake as evidence of hydrothermal or metamorphic processes in their interiors: Geochemical analysis. *Icarus*, *412*, 115999. https://doi.org/10.1016/j.icarus.2024.115999

Gonzalez, Y., Nelson, D. D., Shorter, J. H., McManus, J. B., Dyroff, C., Formolo, M., et al. (2019). Precise measurements of $^{12}CH_2D_2$ by tunable infrared laser direct absorption spectroscopy. *Analytical Chemistry*, *91*(23), 14967–14974. https://doi.org/10.1021/acs.analchem.9b03412

Gruen, D. S., Wang, D. T., Könneke, M., Topçuoğlu, B. D., Stewart, L. C., Goldhammer, T., et al. (2018). Experimental investigation on the controls of clumped isotopologue and hydrogen isotope ratios in microbial methane. *Geochimica et Cosmochimica Acta*, *237*, 339–356. https://doi.org/10.1016/j.gca.2018.06.029

Grundy, W. M., Binzel, R. P., Buratti, B. J., Cook, J. C., Cruikshank, D. P., Dalle Ore, C. M., et al. (2016). Surface compositions across Pluto and Charon. *Science*, *351*(6279), aad9189. https://doi.org/10.1126/science.aad9189

Grundy, W. M., Wong, I., Glein, C. R., Protopapa, S., Holler, B. J., Cook, J. C., et al. (2024). Measurement of D/H and $^{13}C/^{12}C$ ratios in methane ice on Eris and Makemake: Evidence for internal activity. *Icarus*, *411*, 115923. https://doi.org/10.1016/j.icarus.2023.115923

Head, I. M., Jones, D. M., & Larter, S. R. (2003). Biological activity in the deep subsurface and the origin of heavy oil. *Nature*, *426*(6964), 344–352. https://doi.org/10.1038/nature02134

Horibe, Y., & Craig, H. (1995). DH fractionation in the system methane-hydrogen-water. *Geochimica et Cosmochimica Acta*, *59*(24), 5209–5217. https://doi.org/10.1016/0016-7037(95)00391-6

House, C. H., Wong, G. M., Webster, C. R., Flesch, G. J., Franz, H. B., Stern, J. C., et al. (2022). Depleted carbon isotope compositions observed at Gale crater, Mars. *Proceedings of the National Academy of Sciences*, *119*(4), e2115651119. https://doi.org/10.1073/pnas.2115651119

Hudson, R. L., Palumbo, M. E., Strazzulla, G., Moore, M. H., Cooper, J. F., & Sturner, S. J. (2008). Laboratory studies of the chemistry of transneptunian object surface materials. *Solar System Beyond Neptune*, 507–523.

Kelley, D. S., Karson, J. A., Früh-Green, G. L., Yoerger, D. R., Shank, T. M., Butterfield, D. A., et al. (2005). A serpentinite-hosted ecosystem: The lost city hydrothermal field. *Science*, *307*(5714), 1428–1434. https://doi.org/10.1126/science.1102556

Kietäväinen, R., & Purkamo, L. (2015). The origin, source, and cycling of methane in deep crystalline rock biosphere. *Frontiers in Microbiology*, *6*, 146928. https://doi.org/10.3389/fmicb.2015.00725

Klein, F., Grozeva, N. G., & Seewald, J. S. (2019). Abiotic methane synthesis and serpentinization in olivine-hosted fluid inclusions. *Proceedings of the National Academy of Sciences*, *116*(36), 17666–17672. https://doi.org/10.1073/pnas.1907871116

Krasnopolsky, V. A., Maillard, J. P., & Owen, T. C. (2004). Detection of methane in the Martian atmosphere: Evidence for life? *Icarus*, *172*(2), 537–547. https://doi.org/10.1016/j.icarus.2004.07.004

Kueter, N., Schmidt, M. W., Lilley, M. D., & Bernasconi, S. M. (2019). Experimental determination of equilibrium CH_4–CO_2–CO carbon isotope fractionation factors (300–1200°C). *Earth and Planetary Science Letters*, *506*, 64–75. https://doi.org/10.1016/j.epsl.2018.10.021

Labidi, J., Giunta, T., McCollom, T., Sherwood Lollar, B., Leavitt, W. D., & Young, E. D. (2024). Doubly-substituted isotopologues of abiotic methane synthesized in the laboratory, (version 1) [Dataset]. *Interdisciplinary Earth Data Alliance (IEDA)*. https://doi.org/10.60520/IEDA/113221

Labidi, J., Young, E. D., Giunta, T., Kohl, I. E., Seewald, J., Tang, H., et al. (2020). Methane thermometry in deep-sea hydrothermal systems: Evidence for re-ordering of doubly-substituted isotopologues during fluid cooling. *Geochimica et Cosmochimica Acta*, *288*, 248–261. https://doi.org/10.1016/j.gca.2020.08.013

Lalk, E., Pape, T., Gruen, D. S., Kaul, N., Karolewski, J. S., Bohrmann, G., & Ono, S. (2022). Clumped methane isotopologue-based temperature estimates for sources of methane in marine gas hydrates and associated vent gases. *Geochimica et Cosmochimica Acta*, *327*, 276–297. https://doi.org/10.1016/j.gca.2022.04.013

Landwehr, J. M., Coplen, T. B., & Stewart, D. W. (2014). Spatial, seasonal, and source variability in the stable oxygen and hydrogen isotopic composition of tap waters throughout the USA. *Hydrological Processes*, *28*(21), 5382–5422. https://doi.org/10.1002/hyp.10004

Lin, Y., Rumble, D., Young, E. D., Labidi, J., Tu, T., Chen, J., et al. (2023). Diverse origins of gases from mud volcanoes and seeps in tectonically fragmented terrane. *Geochemistry, Geophysics, Geosystems*, *24*(10), e2022GC010791. https://doi.org/10.1029/2022gc010791

Liu, J., Harris, R. L., Ash, J. L., Ferry, J. G., Krause, S. J., Labidi, J., et al. (2023). Reversibility controls on extreme methane clumped isotope signatures from anaerobic oxidation of methane. *Geochimica et Cosmochimica Acta*, *348*, 165–186. https://doi.org/10.1016/j.gca.2023.02.022

Liu, J., Treude, T., Abbasov, O. R., Baloglanov, E. E., Aliyev, A. A., Harris, C. M., et al. (2024). Clumped isotope evidence for microbial alteration of thermogenic methane in terrestrial mud volcanoes. *Geology*, *52*(1), 22–26. https://doi.org/10.1130/g51667.1

McCollom, T. M. (2013). Laboratory simulations of abiotic hydrocarbon formation in Earth's deep subsurface. *Reviews in Mineralogy and Geochemistry*, *75*(1), 467–494. https://doi.org/10.2138/rmg.2013.75.15

McCollom, T. M., Lollar, B. S., Lacrampe-Couloume, G., & Seewald, J. S. (2010). The influence of carbon source on abiotic organic synthesis and carbon isotope fractionation under hydrothermal conditions. *Geochimica et Cosmochimica Acta*, *74*(9), 2717–2740. https://doi.org/10.1016/j.gca.2010.02.008

McCollom, T. M., & Seewald, J. S. (2001). A reassessment of the potential for reduction of dissolved CO_2 to hydrocarbons during serpentinization of olivine. *Geochimica et Cosmochimica Acta*, *65*(21), 3769–3778. https://doi.org/10.1016/s0016-7037(01)00655-x

McCollom, T. M., & Seewald, J. S. (2006). Carbon isotope composition of organic compounds produced by abiotic synthesis under hydrothermal conditions. *Earth and Planetary Science Letters*, *243*(1–2), 74–84. https://doi.org/10.1016/j.epsl.2006.01.027

McCollom, T. M., & Seewald, J. S. (2007). Abiotic synthesis of organic compounds in deep-sea hydrothermal environments. *Chemical Reviews*, *107*(2), 382–401. https://doi.org/10.1021/cr0503660

Miller, H. M., Matter, J. M., Kelemen, P., Ellison, E. T., Conrad, M. E., Fierer, N., et al. (2016). Modern water/rock reactions in Oman hyperalkaline peridotite aquifers and implications for microbial habitability. *Geochimica et Cosmochimica Acta*, *179*, 217–241. https://doi.org/10.1016/j.gca.2016.01.033

Moore, J. M., & McKinnon, W. B. (2021). Geologically diverse Pluto and Charon: Implications for the dwarf planets of the Kuiper Belt. *Annual Review of Earth and Planetary Sciences*, *49*(1), 173–200. https://doi.org/10.1146/annurev-earth-071720-051448

Mumma, M. J., Villanueva, G. L., Novak, R. E., Hewagama, T., Bonev, B. P., DiSanti, M. A., et al. (2009). Strong release of methane on Mars in northern summer 2003. *Science*, *323*(5917), 1041–1045. https://doi.org/10.1126/science.1165243

NASEM. (2022). Origins, worlds, and life: A decadal strategy for planetary science and astrobiology 2023–2032.

Neveu, M., Hays, L. E., Voytek, M. A., New, M. H., & Schulte, M. D. (2018). The ladder of life detection. *Astrobiology*, *18*(11), 1375–1402. https://doi.org/10.1089/ast.2017.1773

Niemann, H. B., Atreya, S. K., Bauer, S. J., Carignan, G. R., Demick, J. E., Frost, R. L., et al. (2005). The abundances of constituents of Titan's atmosphere from the GCMS instrument on the Huygens probe. *Nature*, *438*(7069), 779–784. https://doi.org/10.1038/nature04122

Nothaft, D. B., Templeton, A. S., Boyd, E. S., Matter, J. M., Stute, M., Paukert Vankeuren, A. N., & Team, O. D. P. S. (2021). Aqueous geochemical and microbial variation across discrete depth intervals in a peridotite aquifer assessed using a packer system in the Samail Ophiolite, Oman. *Journal of Geophysical Research: Biogeosciences*, *126*(9), e2021JG006319. https://doi.org/10.1029/2021jg006319

Owen, T. C., Roush, T. L., Cruikshank, D. P., Elliot, J. L., Young, L. A., De Bergh, C., et al. (1993). Surface ices and the atmospheric composition of Pluto. *Science*, *261*(5122), 745–748. https://doi.org/10.1126/science.261.5122.745

Pester, N. J., Conrad, M. E., Knauss, K. G., & DePaolo, D. J. (2018). Kinetics of D/H isotope fractionation between molecular hydrogen and water. *Geochimica et Cosmochimica Acta*, *242*, 191–212. https://doi.org/10.1016/j.gca.2018.09.015

Proskurowski, G., Lilley, M. D., Seewald, J. S., Früh-Green, G. L., Olson, E. J., Lupton, J. E., et al. (2008). Abiogenic hydrocarbon production at Lost City hydrothermal field. *Science*, *319*(5863), 604–607. https://doi.org/10.1126/science.1151194

Qi, Y., Yang, J., Duan, X., Zhu, Y.-A., Chen, D., & Holmen, A. (2014). Discrimination of the mechanism of CH_4 formation in Fischer–Tropsch synthesis on Co catalysts: A combined approach of DFT, kinetic isotope effects and kinetic analysis. *Catalysis Science & Technology*, *4*(10), 3534–3543. https://doi.org/10.1039/c4cy00566j

Röckmann, T., Popa, M. E., Krol, M. C., & Hofmann, M. E. G. (2016). Statistical clumped isotope signatures. *Scientific Reports*, *6*, 1–14. https://doi.org/10.1038/srep31947

Rolston, J. H., Den Hartog, J., & Butler, J. P. (1976). The deuterium isotope separation factor between hydrogen and liquid water. *Journal of Physical Chemistry A*, *80*(10), 1064–1067. https://doi.org/10.1021/j100551a008

Sauterey, B., Charnay, B., Affholder, A., Mazevet, S., & Ferrière, R. (2022). Early Mars habitability and global cooling by H_2-based methanogens. *Nature Astronomy*, *6*(11), 1263–1271. https://doi.org/10.1038/s41550-022-01786-w

Seewald, J. S., Zolotov, M. Y., & McCollom, T. M. (2006). Experimental investigation of single carbon compounds under hydrothermal conditions. *Geochimica et Cosmochimica Acta*, *70*(2), 446–460. https://doi.org/10.1016/j.gca.2005.09.002

Seyfried, W. E., Jr., Janecky, D. R., & Berndt, M. E. (1987). Rocking autoclaves for hydrothermal experiments II. The flexible reaction-cell system. *Hydrothermal Experimental Techniques*, *23*, 216–239.

Sherwood Lollar, B., Frape, S. K., Weise, S. M., Fritz, P., Macko, S. A., & Welhan, J. A. (1993). Abiogenic methanogenesis in crystalline rocks. *Geochimica et Cosmochimica Acta*, *57*(23–24), 5087–5097. https://doi.org/10.1016/0016-7037(93)90610-9

Sherwood Lollar, B., Lacrampe-Couloume, G., Slater, G. F., Ward, J., Moser, D. P., Gihring, T. M., et al. (2006). Unravelling abiogenic and biogenic sources of methane in the Earth's deep subsurface. *Chemical Geology*, *226*(3–4), 328–339. https://doi.org/10.1016/j.chemgeo.2005.09.027

Sherwood Lollar, B., Lacrampe-Couloume, G., Voglesonger, K., Onstott, T. C., Pratt, L. M., & Slater, G. F. (2008). Isotopic signatures of CH_4 and higher hydrocarbon gases from Precambrian Shield sites: A model for abiogenic polymerization of hydrocarbons. *Geochimica et Cosmochimica Acta*, *72*(19), 4778–4795. https://doi.org/10.1016/j.gca.2008.07.004

Sherwood Lollar, B., Westgate, T. D., Ward, J. A., Slater, G. F., & Lacrampe-Couloume, G. (2002). Abiogenic formation of alkanes in the Earth's crust as a minor source for global hydrocarbon reservoirs. *Nature*, *416*(6880), 522–524. https://doi.org/10.1038/416522a

Shuai, Y., Etiope, G., Zhang, S., Douglas, P. M. J., Huang, L., & Eiler, J. M. (2018). Methane clumped isotopes in the Songliao Basin (China): New insights into abiotic vs. biotic hydrocarbon formation. *Earth and Planetary Science Letters*, *482*, 213–221. https://doi.org/10.1016/j.epsl.2017.10.057

Stolper, D. A., Lawson, M., Davis, C. L., Ferreira, A. A., Neto, E. V. S., Ellis, G. S., et al. (2014). Formation temperatures of thermogenic and biogenic methane. *Science*, *344*(6191), 1500–1503. https://doi.org/10.1126/science.1254509

Strobel, D. F. (1974). The photochemistry of hydrocarbons in the atmosphere of Titan. *Icarus*, *21*(4), 466–470. https://doi.org/10.1016/0019-1035(74)90149-3

Taenzer, L., Labidi, J., Masterson, A. L., Feng, X., Rumble, III, D., Young, E. D., & Leavitt, W. D. (2020). Low $\Delta^{12}CH_2D_2$ values in microbialgenic methane result from combinatorial isotope effects. *Geochimica et Cosmochimica Acta*, *285*, 225–236. https://doi.org/10.1016/j.gca.2020.06.026

Takai, K., Nakamura, K., Toki, T., Tsunogai, U., Miyazaki, M., Miyazaki, J., et al. (2008). Cell proliferation at ^{122}C and isotopically heavy CH_4 production by a hyperthermophilic methanogen under high-pressure cultivation. *Proceedings of the National Academy of Sciences*, *105*(31), 10949–10954. https://doi.org/10.1073/pnas.0712334105

Taran, Y. A., Kliger, G. A., Cienfuegos, E., & Shuykin, A. N. (2010). Carbon and hydrogen isotopic compositions of products of open-system catalytic hydrogenation of CO_2: Implications for abiogenic hydrocarbons in Earth's crust. *Geochimica et Cosmochimica Acta*, *74*(21), 6112–6125. https://doi.org/10.1016/j.gca.2010.08.012

Thompson, M. A., Krissansen-Totton, J., Wogan, N., Telus, M., & Fortney, J. J. (2022). The case and context for atmospheric methane as an exoplanet biosignature. *Proceedings of the National Academy of Sciences*, *119*(14), e2117933119. https://doi.org/10.1073/pnas.2117933119

Turner, A. C., Pester, N. J., Bill, M., Conrad, M. E., Knauss, K. G., & Stolper, D. A. (2022). Experimental determination of hydrogen isotope exchange rates between methane and water under hydrothermal conditions. *Geochimica et Cosmochimica Acta*, *329*, 231–255. https://doi.org/10.1016/j.gca.2022.04.029

Tyler, G. L., Eshleman, V. R., Anderson, J. D., Levy, G. S., Lindal, G. F., Wood, G. E., & Croft, T. A. (1981). Radio science investigations of the Saturn system with Voyager 1: Preliminary results. *Science*, *212*(4491), 201–206. https://doi.org/10.1126/science.212.4491.201

Waite, J. H., Glein, C. R., Perryman, R. S., Teolis, B. D., Magee, B. A., Miller, G., et al. (2017). Cassini finds molecular hydrogen in the Enceladus plume: Evidence for hydrothermal processes. *Science*, *356*(6334), 155–159. https://doi.org/10.1126/science.aai8703

Waite, J. H., Jr., Combi, M. R., Ip, W.-H., Cravens, T. E., McNutt, R. L., Jr., Kasprzak, W., et al. (2006). Cassini ion and neutral mass spectrometer: Enceladus plume composition and structure. *Science*, *311*(5766), 1419–1422. https://doi.org/10.1126/science.1121290

Wang, D. T., Gruen, D. S., Lollar, B. S., Hinrichs, K.-U., Stewart, L. C., Holden, J. F., et al. (2015). Nonequilibrium clumped isotope signals in microbial methane. *Science*, *348*(6233), 428–431. https://doi.org/10.1126/science.aaa4326

Wang, D. T., Reeves, E. P., McDermott, J. M., Seewald, J. S., & Ono, S. (2018). Clumped isotopologue constraints on the origin of methane at seafloor hot springs. *Geochimica et Cosmochimica Acta*, *223*, 141–158. https://doi.org/10.1016/j.gca.2017.11.030

Wang, W., Wang, S., Ma, X., & Gong, J. (2011). Recent advances in catalytic hydrogenation of carbon dioxide. *Chemical Society Reviews*, *40*(7), 3703–3727. https://doi.org/10.1039/c1cs15008a

Warr, O., Young, E. D., Giunta, T., Kohl, I. E., Ash, J. L., & Lollar, B. S. (2021). High-resolution, long-term isotopic and isotopologue variation identifies the sources and sinks of methane in a deep subsurface carbon cycle. *Geochimica et Cosmochimica Acta*, *294*, 315–334. https://doi.org/10.1016/j.gca.2020.12.002

Webster, C. R., Mahaffy, P. R., Atreya, S. K., Flesch, G. J., Mischna, M. A., Meslin, P.-Y., et al. (2015). Mars methane detection and variability at Gale crater. *Science*, *347*(6220), 415–417. https://doi.org/10.1126/science.1261713

Welhan, J. A., & Craig, H. (1979). Methane and hydrogen in East Pacific Rise hydrothermal fluids. *Geophysical Research Letters*, *6*(11), 829–831. https://doi.org/10.1029/GL006i011p00829

Xie, H., Dong, G., Formolo, M., Lawson, M., Liu, J., Cong, F., et al. (2021). The evolution of intra-and inter-molecular isotope equilibria in natural gases with thermal maturation. *Geochimica et Cosmochimica Acta*, *307*, 22–41. https://doi.org/10.1016/j.gca.2021.05.012

Yanez, M. D., LaRowe, D. E., Cable, M. L., & Amend, J. P. (2024). Energy yields for acetylenotrophy on Enceladus and titan. *Icarus*, *411*, 115969. https://doi.org/10.1016/j.icarus.2024.115969

Yeung, L. Y. (2016). Combinatorial effects on clumped isotopes and their significance in biogeochemistry. *Geochimica et Cosmochimica Acta*, *172*, 22–38. https://doi.org/10.1016/j.gca.2015.09.020

Young, E. D. (2019). A two-dimensional perspective on CH4 isotope clumping: Distinguishing process from source. In *Deep carbon, 388414*.

Young, E. D., Kohl, I. E., Lollar, B. S., Etiope, G., Rumble, III, D., Li, S., et al. (2017). The relative abundances of resolved $^{12}CH_2D_2$ and $^{13}CH_3D$ and mechanisms controlling isotopic bond ordering in abiotic and biotic methane gases. *Geochimica et Cosmochimica Acta*, *203*, 235–264. https://doi.org/10.1016/j.gca.2016.12.041

Young, E. D., Rumble, III, D., Freedman, P., & Mills, M. (2016). A large-radius high-mass-resolution multiple-collector isotope ratio mass spectrometer for analysis of rare isotopologues of O_2, N_2, CH_4 and other gases. *International Journal of Mass Spectrometry*, *401*, 1–10. https://doi.org/10.1016/j.ijms.2016.01.006